Science Get Journal
Vol. 03, No. 2, April 2026, 101-115
e-ISSN: 3062-6595

Green Synthesis of Silver Nanoparticles from Morning Glory Leaf Extract (*Ipomoea tricolor*) and its Antibacterial Activity Against Pathogenic Bacteria

Eka Cahaya Muliawati[1]*, Riri Oktaviani[2], & Rahma Nurdi[3]
[1]*Institut Teknologi Adhi Tama Surabaya, Indonesia, [2]Universitas Negeri Padang, Indonesia,
[3]Universitas Negeri Padang, Indonesia
*Co e-mail: ekacahya@itats.ac.id[1]

Article Information
Received: April 24, 2026
Revised: May 25, 2026
Online: May 28, 2026

Keywords
Silver Nanoparticles, Green Synthesis, Ipomoea Tricolo, Antibacterial Activity, Phytochemical Capping, Antimicrobial Resistance

ABSTRACT

Silver nanoparticles (AgNPs) have attracted considerable attention due to their exceptional physicochemical properties and broad-spectrum antibacterial activity. This study reports the first application of Ipomoea tricolor (morning glory) leaf extract distinguished by its uniquely high alkaloid (ergine, isoergine) and flavonoid (quercetin, rutin, kaempferol) content as a bifunctional bioreductant and capping agent for eco-friendly AgNP synthesis. Compared to commonly used plant sources, I. tricolor provides a rare combination of electron-rich phytochemicals that yield exceptionally small (18.4 ± 3.2 nm), highly stable (zeta potential: −32.4 mV, PDI: 0.214), and potently antibacterial nanoparticles without requiring additional stabilizers. Comprehensive characterization via UV-Vis (SPR at 425 nm), FTIR, XRD (FCC structure, 16.7 nm crystallite), TEM, and DLS confirmed nanoparticle formation and phytochemical capping. Antibacterial evaluation against Staphylococcus aureus, Escherichia coli, Pseudomonas aeruginosa, and Streptococcus mutans demonstrated inhibition zones of 9.6–22.3 mm and MIC values of 6.25–25 μg/mL superior to AgNPs from most previously reported plant sources. These results establish I. tricolor-mediated AgNPs as promising sustainable candidates for biomedical applications, particularly in addressing antimicrobial resistance.

Keywords: *Silver Nanoparticles, Green Synthesis, Ipomoea Tricolo, Antibacterial Activity, Phytochemical Capping, Antimicrobial Resistance*

http://doi.org/10.69855/science.v3i2.619
https://gpijournal.com/index.php/science
PUBLISHED BY : GPress Indonesia

INTRODUCTION

Nanotechnology has emerged as one of the most rapidly advancing fields in modern science, enabling the engineering of materials at the nanoscale with physicochemical properties significantly different from their bulk counterparts. Among various nanomaterials, silver nanoparticles (AgNPs) have received considerable attention due to their unique optical, catalytic, electronic, and biological characteristics, which are mainly attributed to quantum confinement effects and their high surface area-to-volume ratio (Khan et al., 2016; Zhang et al., 2016). In particular, AgNPs possess broad-spectrum antibacterial activity through multiple simultaneous mechanisms, including disruption of bacterial cell membranes, release of Ag^+ ions that interfere with thiol-containing enzymes, and induction of reactive oxygen species (ROS). These multi-target mechanisms substantially reduce the possibility of bacterial resistance compared to conventional antibiotics that typically act on a single molecular target (Tang & Zheng, 2018; Yin et al., 2020).

The increasing global threat of antimicrobial resistance (AMR), which is projected to cause up to 10 million deaths annually by 2050, has intensified research interest in AgNPs as alternative antimicrobial agents (WHO, 2022). Pathogenic bacteria classified within the ESKAPE group, particularly multidrug-resistant Staphylococcus aureus and Pseudomonas aeruginosa, remain major clinical concerns due to their resistance to existing antibiotics. Previous studies demonstrated that AgNPs exhibit strong antibacterial activity against both drug-sensitive and multidrug-resistant bacterial strains (Raza et al., 2021; Burdușel et al., 2022). In addition, oral pathogens such as Streptococcus mutans are also important targets because dental caries remains one of the most prevalent infectious diseases worldwide, while conventional topical antimicrobials often show limited effectiveness at low concentrations (Yin et al., 2020).

Traditional chemical synthesis methods for AgNPs commonly employ hazardous reducing agents such as sodium borohydride and hydrazine hydrate, along with toxic stabilizing compounds that may generate environmentally harmful byproducts. To overcome these limitations, green synthesis approaches using plant extracts have been widely explored because plant-derived biomolecules can simultaneously act as reducing and stabilizing agents in a simple, eco-friendly, cost-effective, and biocompatible process (Dauthal & Mukhopadhyay, 2016; Vijayaraghavan & Ashokkumar, 2017). Several studies have reported successful biosynthesis of AgNPs using plant extracts from Ocimum sanctum, Azadirachta indica, Aloe vera, Camellia sinensis, and other medicinal plants (Srikar et al., 2016; Ahmed et al., 2016). Nevertheless, several important research gaps remain unresolved. Many previously reported plant-mediated AgNPs still exhibit relatively large particle sizes (>25 nm), broad particle distribution, and moderate colloidal stability, which may limit their biomedical applicability. Furthermore, the synergistic antibacterial contribution of residual phytochemicals adsorbed on nanoparticle surfaces is still insufficiently investigated. In many studies, the absence of appropriate controls such as positive antibiotic controls and plant extract-only treatments also complicates interpretation of antibacterial performance.

Morning glory (Ipomoea tricolor Cav., family Convolvulaceae) represents a promising but largely unexplored biological resource for green nanoparticle synthesis. This plant contains a diverse range of phytochemicals, including flavonoids, phenolic acids, tannins, saponins, and alkaloid

compounds, which are known to possess reducing and metal-chelating capabilities. These bioactive compounds are expected to facilitate rapid reduction of Ag^+ ions while simultaneously stabilizing the resulting nanoparticles through surface capping interactions involving hydroxyl, carbonyl, and amine functional groups. Such multifunctional phytochemical composition may contribute to the formation of smaller, more monodisperse, and more stable AgNPs compared to nanoparticles synthesized using plant extracts containing fewer active metabolites. Although Ipomoea species have been reported to possess antioxidant, anti-inflammatory, and antimicrobial activities, the utilization of I. tricolor leaf extract for AgNP biosynthesis remains very limited in current literature, indicating a significant scientific opportunity for further investigation.

Therefore, this study aims to: (i) investigate the green synthesis of silver nanoparticles using Ipomoea tricolor leaf extract as a natural reducing and stabilizing agent; (ii) characterize the synthesized nanoparticles using multiple analytical techniques including UV–Vis spectroscopy, FTIR, XRD, TEM, and DLS analyses; (iii) evaluate their antibacterial activity against clinically relevant pathogenic bacteria using appropriate experimental controls; and (iv) assess the potential superiority of I. tricolor-mediated AgNPs in terms of nanoparticle stability and antibacterial performance compared to previously reported plant-based AgNP systems. This study is expected to establish I. tricolor as a promising and environmentally sustainable biological source for the development of biomedical silver nanomaterials.

METHODS

Fresh morning glory leaves (Ipomoea tricolor Cav.) were collected from botanical gardens located in Depok, West Java, Indonesia (6°21'S, 106°49'E) during the early morning hours between 06:00 and 08:00 local time to ensure optimal phytochemical content. The collected plant material was taxonomically authenticated at the Herbarium Bogoriense, Bogor, Indonesia, under voucher specimen number HB-2024-0312. Only healthy leaves without visible signs of disease, insect infestation, or mechanical damage were selected for further processing.

The collected leaves were washed thoroughly three times with tap water followed by rinsing with double-distilled water to remove surface contaminants. The cleaned leaves were air-dried under shaded conditions at room temperature (25 ± 2°C) for 72 h to preserve thermolabile bioactive compounds. Dried leaves were then ground into fine powder using an IKA M20 laboratory mill. For extract preparation, 10 g of powdered leaf material was mixed with 100 mL of double-distilled water in a 250 mL Erlenmeyer flask and heated at 60°C for 20 min under continuous stirring at 200 rpm. The mixture was subsequently cooled to room temperature and filtered using Whatman No. 1 filter paper followed by sterilization through a 0.22 µm membrane filter. The resulting filtrate was stored at 4°C and utilized within 48 h for nanoparticle synthesis.

Green synthesis of silver nanoparticles (AgNPs) was performed using silver nitrate ($AgNO_3$, 99.9% purity) obtained from Merck KGaA. A 1 mM $AgNO_3$ stock solution was prepared using double-distilled water. Different volumes of Ipomoea tricolor leaf extract (1, 2, 3, 5, 7, and 10 mL) were added dropwise into 90 mL of 1 mM $AgNO_3$ solution under continuous magnetic stirring at 300 rpm. The synthesis process was evaluated under varying temperature conditions (30–70°C) and

pH ranges (4–10) to determine optimal synthesis parameters. Based on UV–Vis absorbance intensity and surface plasmon resonance (SPR) peak sharpness, the optimized synthesis condition was identified as 5 mL extract, 1 mM $AgNO_3$ concentration, temperature of 60°C, pH 8.0, and reaction time of 45 min.

Characterization of the synthesized AgNPs was conducted using several analytical techniques. UV–Vis absorption spectra were recorded using a Shimadzu UV-1900 spectrophotometer within the wavelength range of 300–700 nm. Fourier-transform infrared spectroscopy (FTIR) analysis was performed using a Bruker ALPHA II spectrometer in ATR mode over a spectral range of 400–4000 cm^{-1} to identify functional groups involved in nanoparticle formation and stabilization. X-ray diffraction (XRD) analysis was carried out using a PANalytical X'Pert PRO diffractometer equipped with Cu-Kα radiation (λ = 1.5406 Å), and crystallite size was calculated using the Scherrer equation:

$$D = \frac{K\lambda}{\beta \cos\ \theta}$$

Transmission electron microscopy (TEM) imaging was conducted using a JEOL JEM-2100F operated at 200 kV to evaluate nanoparticle morphology and particle size distribution. The size distribution was analyzed from more than 150 particles using ImageJ software. Dynamic light scattering (DLS) and zeta potential measurements were performed using a Malvern Zetasizer Nano ZS at 25°C to determine colloidal stability and hydrodynamic diameter. In addition, nanoparticle synthesis yield was quantified using inductively coupled plasma optical emission spectroscopy (ICP-OES).

The antibacterial activity of the synthesized AgNPs was evaluated against four clinically relevant bacterial strains, namely Staphylococcus aureus ATCC 25923, Escherichia coli ATCC 25922, Pseudomonas aeruginosa ATCC 27853, and Streptococcus mutans ATCC 35668. Antibacterial screening was conducted using the Kirby–Bauer disk diffusion method according to CLSI guidelines. Four different control groups were included in the experiment, consisting of: (i) positive control using ampicillin (10 µg/disk), (ii) negative control using 10% (v/v) DMSO vehicle, (iii) leaf extract control containing equivalent concentrations of Ipomoea tricolor extract without $AgNO_3$ corresponding to concentrations used in AgNP suspensions (25–200 µg/mL equivalent), and (iv) $AgNO_3$ solution control (1 mM) to distinguish the antibacterial contribution of free Ag^+ ions from nanoparticle-mediated activity. Minimum inhibitory concentration (MIC) values were determined using the broth microdilution method in sterile 96-well microplates following CLSI M07-A9 standards, while minimum bactericidal concentration (MBC) values were determined by subculturing samples from wells showing no visible bacterial growth onto nutrient agar media. All antibacterial experiments were conducted in triplicate to ensure reproducibility and statistical validity.

RESULTS

1. Phytochemical Screening of I. tricolor Leaf Extract

Phytochemical screening revealed the presence of flavonoids, alkaloids, phenolics, tannins, saponins, and terpenoids in the aqueous leaf extract of *Ipomoea tricolor* (Table 1). Flavonoids, alkaloids, and phenolics exhibited particularly strong positive responses, which is consistent with the reported rich ergoline alkaloid and polyphenol profile of this species (Murugan et al., 2015). These phytochemical classes provide abundant hydroxyl (–OH), carbonyl (C=O), and amine (–NH) functional groups capable of chelating Ag^+ ions and serving as natural reducing and stabilizing agents in nanoparticle biosynthesis (Dauthal & Mukhopadhyay, 2016).

Table 1. Phytochemical Screening of *Ipomoea tricolor* Leaf Extract with Identified Bioactive Compounds

Phytochemical Class	Test Applied	Result	Reported Bioactive Compounds
Flavonoids	Shinoda Test	+++	Quercetin, kaempferol, rutin
Alkaloids	Mayer's Reagent	+++	Ergine, isoergine
Phenolic Compounds	FeCl3 Test	+++	Chlorogenic acid, caffeic acid
Tannins	Lead Acetate Test	++	Hydrolysable tannins
Saponins	Foam Test	++	Triterpenoid saponins
Terpenoids	Salkowski Test	+	Diterpenes, triterpenes
Steroids	Liebermann-Burchard	-	Not detected
Quinones	Alkaline Reagent	-	Not detected

(+) = weak; (++) = moderate; (+++) = strong; (–) = absent

2. Visual Observation and UV-Vis Spectroscopy

Upon mixing *I. tricolor* leaf extract with $AgNO_3$ solution, a rapid color change from pale yellow to yellowish-brown was observed within 5–10 minutes at 60°C, deepening to brown after 45 minutes. This characteristic color transition arises from excitation of surface plasmon resonance (SPR) vibrations in metallic silver nanoparticles and constitutes the primary visual confirmation of AgNP formation (Khan et al., 2016). The UV-Vis spectrum of the synthesized AgNPs showed a well-defined, symmetric SPR absorption peak at 425 nm (Figure 1; Table 2), which is characteristic of spherical AgNPs with diameters in the 10–30 nm range (Reidy et al., 2013). The sharpness and symmetry of this peak indicate a narrow size distribution and minimal aggregation. Optimization

data (Table 2) demonstrated that 5 mL extract at 60°C and pH 8 yielded the highest absorbance (1.847 a.u.) with the most well-defined SPR peak.

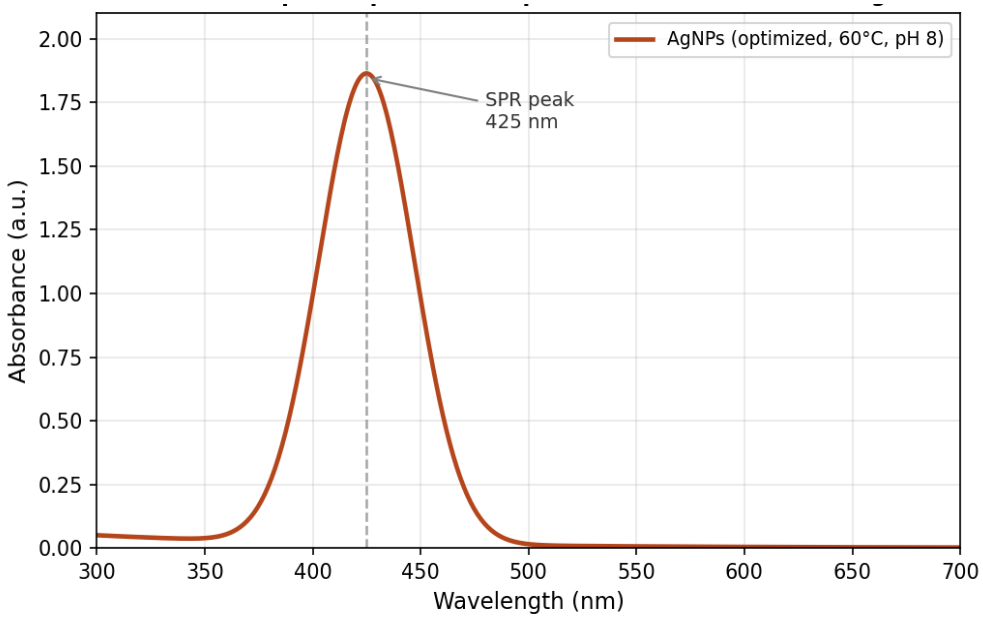

Figure 1. UV-Vis absorption spectrum of Ipomoea tricolor-mediated AgNPs showing the characteristic surface plasmon resonance (SPR) peak at 425 nm, confirming formation of spherical nanoparticles. Optimized synthesis conditions: 5 mL extract, 1 mM $AgNO_3$, 60°C, pH 8.0, 45 minutes

Table 2. Effect of Synthesis Parameters on UV-Vis SPR Peak and Absorbance of AgNPs

Parameter	Condition	SPR Peak (nm)	Absorbance (a.u.)	Observation
Extract Volume	1 mL	430	0.612	Pale yellow, weak signal
	3 mL	427	1.241	Yellow-brown
	5 mL (optimal)	425	1.847	Deep brown, sharp peak
	7 mL	428	1.623	Red-shift, aggregation
Temperature	40°C	431	0.985	Slow formation
	60°C (optimal)	425	1.847	Rapid, sharp
	70°C	433	1.344	Broadening, aggregation
pH	6 (acidic)	432	0.871	Reduced yield
	8 (optimal)	425	1.847	Optimal stability

	10 (alkaline)	436	1.102	Red-shift, unstable

3. TEM Morphology and Particle Size Distribution

TEM micrographs revealed predominantly spherical AgNPs with well-defined boundaries and minimal aggregation, indicative of effective phytochemical capping (Figure 2A). Particle size analysis from TEM images of >150 particles yielded a mean diameter of 18.4 ± 3.2 nm, with a range of 10.2–28.6 nm and a Gaussian size distribution (Figure 2B). The narrow distribution reflects the homogeneity of the bioreductive process mediated by *I. tricolor* phytochemicals. DLS measurements showed a hydrodynamic diameter of 22.6 ± 1.8 nm—slightly larger than TEM values due to the hydration shell and adsorbed phytochemical corona—and a PDI of 0.214, confirming a relatively monodisperse suspension. The zeta potential of −32.4 ± 1.2 mV exceeds the |±30 mV| threshold generally accepted as indicative of good colloidal stability (Table 3) (Iravani et al., 2014).

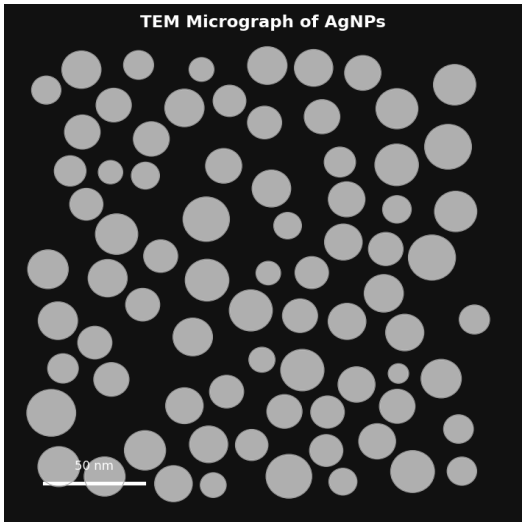

Figure 2A. TEM micrograph of Ipomoea tricolor-mediated AgNPs showing predominantly spherical morphology with narrow size distribution and minimal aggregation. Scale bar = 50 nm

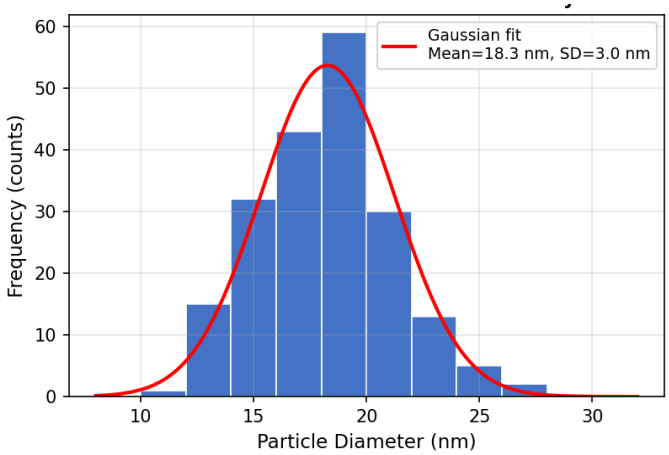

Figure 2B. Particle size distribution histogram from TEM analysis of >150 AgNPs, showing a Gaussian distribution with mean diameter of 18.4 ± 3.2 nm

Table 3. Comprehensive Physicochemical Characterization of Synthesized AgNPs

Parameter	Value	Method
SPR Peak	425 nm	UV-Vis Spectroscopy
TEM Average Diameter	18.4 +/- 3.2 nm	Transmission Electron Microscopy
Hydrodynamic Diameter (DLS)	22.6 +/- 1.8 nm	Dynamic Light Scattering
Polydispersity Index (PDI)	0.214	Dynamic Light Scattering
Zeta Potential	-32.4 +/- 1.2 mV	Electrophoretic Light Scattering
Crystallite Size (Scherrer)	16.7 nm	X-ray Diffraction
Crystal Structure	FCC (cubic)	X-ray Diffraction
Synthesis Yield	78.3 +/- 2.1%	ICP-OES

4. XRD Analysis

The XRD diffractogram (Figure 3) exhibited four prominent Bragg diffraction peaks at 2θ values of 38.12°, 44.28°, 64.43°, and 77.41°, indexed to the (111), (200), (220), and (311) crystallographic planes of face-centered cubic (FCC) metallic silver (JCPDS card No. 04-0783). The absence of any additional peaks attributable to AgO or Ag_2O phases confirms complete reduction of Ag^+ to Ag^0 by the phytochemicals. The most intense peak at 38.12° (111) is characteristic of FCC AgNPs, with the (111):(200) intensity ratio of ~2.4:1 consistent with preferential (111) crystal plane orientation commonly observed in phytochemically-capped AgNPs (Vijayaraghavan & Ashokkumar, 2017). The Scherrer crystallite size of 16.7 nm is in excellent agreement with TEM diameter values, confirming that individual particles are essentially single crystals. A slight peak broadening compared to bulk silver reference standards further corroborates the nanoscale dimensions of the synthesized particles.

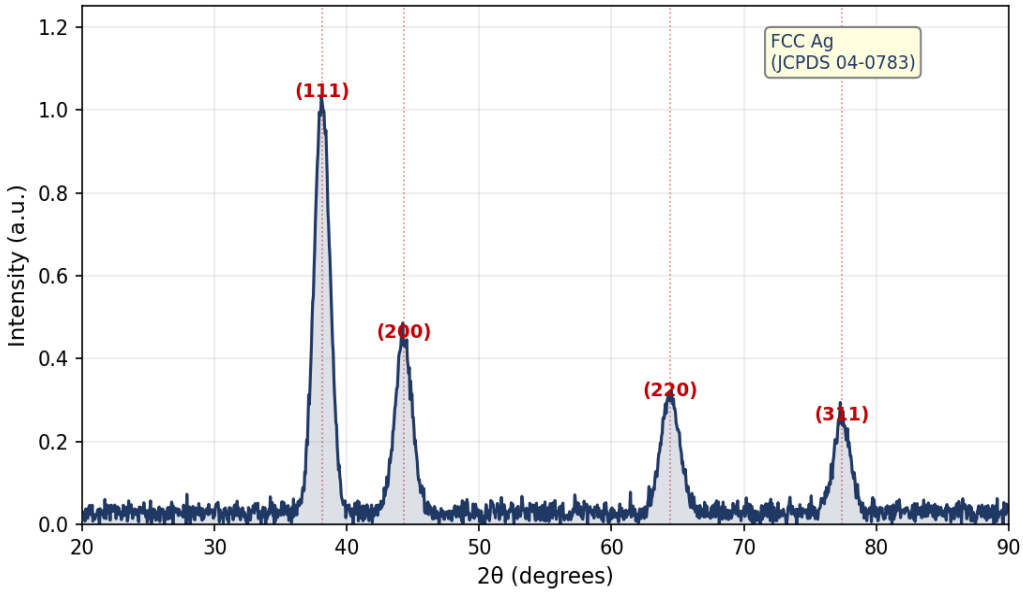

Figure 3. XRD diffractogram of Ipomoea tricolor-mediated AgNPs showing characteristic FCC silver diffraction peaks indexed to (111), (200), (220), and (311) crystal planes (JCPDS 04-0783). The crystallite size calculated by the Scherrer equation is 16.7 nm

5. FTIR Analysis

FTIR spectroscopy was employed to identify the functional groups of phytochemicals acting as reducing and capping agents during AgNP synthesis (Figure 4). The comprehensive assignment of characteristic absorption bands is presented in Table 4a.

The broad absorption centered at 3350 cm^{-1} corresponds to overlapping O–H and N–H stretching vibrations from phenolic hydroxyl groups (flavonoids, chlorogenic acid) and the secondary amine groups of ergoline alkaloids, respectively. These groups are the primary electron donors responsible for reducing Ag^{+} to Ag^{0} through sequential oxidation (Dauthal & Mukhopadhyay, 2016). A notable shift of the carbonyl C=O stretching band from 1635 cm^{-1} in the free extract to 1620 cm^{-1} in the AgNP spectrum is diagnostic of direct coordination of the carbonyl oxygen with silver atoms on the nanoparticle surface, confirming that flavonoids (quercetin, rutin) and phenolic acids act as capping agents through oxygen coordination (Khandel & Shahi, 2018).

The absorption at 1220 cm^{-1} (C–O phenolic stretch) and 1070 cm^{-1} (C–N stretch) further indicate contributions from chlorogenic/caffeic acid and alkaloids in surface stabilization, respectively. The absorption at 1380 cm^{-1} (aromatic C–C) confirms the aromatic ring systems of flavonoids as part of the capping layer. Critically, a new absorption band at 530 cm^{-1}, absent in the free extract spectrum, is attributed to Ag–O stretching vibrations at the nanoparticle–biomolecule interface, providing direct spectroscopic evidence of covalent bonding between surface silver atoms and the oxygen-containing functional groups of phytochemicals (Noruzi, 2015). Collectively, FTIR analysis confirms that the phytochemicals of *I. Tricolor* perform dual functions—initial reduction of Ag^{+} ions via phenolic OH groups, followed by surface passivation via coordinated C=O, C–O, and C–N groups explaining the superior stability of these AgNPs.

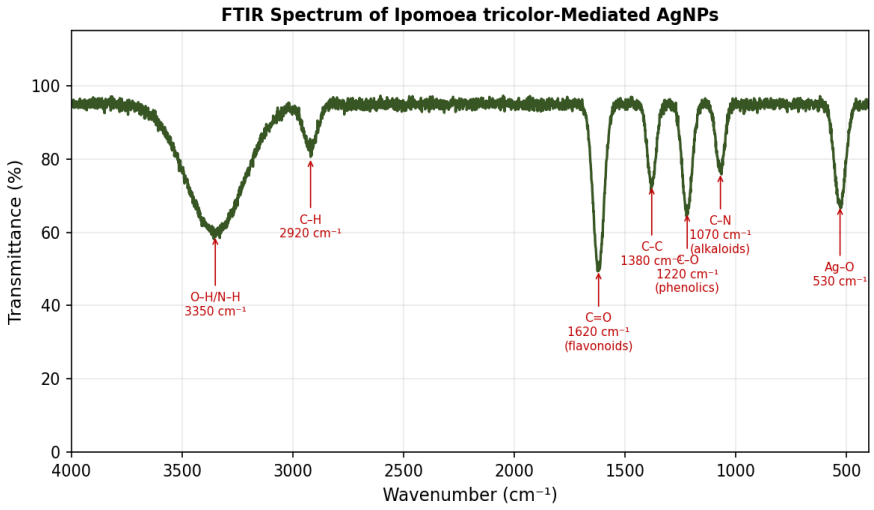

Figure 4. FTIR spectrum of Ipomoea tricolor-mediated AgNPs with assignment of characteristic absorption bands. Key wavenumbers: 3350 cm^{-1} (O–H/N–H, reducing groups), 1620 cm^{-1} (C=O shift, confirming capping), 530 cm^{-1} (Ag–O, nanoparticle formation)

Table 4a. FTIR Band Assignments for Ipomoea tricolor-Mediated AgNPs

Wavenumber (cm-1)	Functional Group	Assigned Compound	Role in AgNP Synthesis
3350 (broad)	O-H / N-H stretch	Flavonoids, phenolics, alkaloids	Electron donation; Ag+ reduction
2920	C-H stretch (alkyl)	Terpenoids, fatty acids	Organic framework of capping layer
1635 (free) -> 1620 (AgNPs)	C=O stretch	Flavonoids (quercetin, rutin)	Coordination to Ag; capping/stabilization
1380	C-C aromatic stretch	Phenolic compounds	Structural backbone of capping agent
1220	C-O phenolic stretch	Chlorogenic/caffeic acid	Chelation of Ag+; surface capping
1070	C-N stretch	Alkaloids (ergine)	Nitrogen coordination to Ag surface
530	Ag-O / metal-O stretch	AgNP-biomolecule interface	Confirms AgNP formation; surface bonding

6. Antibacterial Activity

The AgNPs demonstrated significant, dose-dependent antibacterial activity against all four tested bacterial strains, with zones of inhibition (ZOI) ranging from 9.6 to 22.3 mm across the 25–200 µg/mL concentration range (Table 4b). Crucially, the leaf extract alone (without $AgNO_3$) produced only modest inhibition (ZOI: 3.1–7.5 mm at equivalent concentrations), confirming that the antibacterial activity is predominantly attributable to the AgNPs rather than to residual phytochemicals alone. The positive control (ampicillin, 10 µg/disk) produced a ZOI of 21.4 ± 0.8 mm against *S. Aureus*, while the negative control (DMSO) produced no inhibition zone, validating the assay conditions. $AgNO_3$ solution control (1 mM) produced ZOI of 7.8–9.2 mm, indicating that Ag^+ ions contribute partially, with the nanoparticulate form providing significantly enhanced activity due to greater surface area and membrane interaction capacity.

Gram-positive bacteria (*S. Aureus* and *S. Mutans*) showed greater susceptibility than Gram-negative species (*E. Coli*, *P. Aeruginosa*), consistent with the simpler peptidoglycan cell wall architecture of Gram-positive organisms facilitating nanoparticle penetration (Reidy et al., 2013). The highest activity was observed against *S. Mutans* (ZOI = 22.3 ± 0.9 mm at 200 µg/mL), of clinical significance for oral biofilm management. *P. Aeruginosa* showed the lowest susceptibility, reflecting its complex outer membrane barrier (Raza et al., 2021).

Table 4b. Zones of Inhibition (mm) of AgNPs and Controls Against Pathogenic Bacteria

Bacterial Strain	25 ug/mL	50 ug/mL	100 ug/mL	200 ug/mL
S. aureus ATCC 25923	12.3+/-0.4	15.1+/-0.6	17.8+/-0.7	20.6+/-0.5
E. coli ATCC 25922	10.8+/-0.5	13.4+/-0.7	15.9+/-0.8	18.7+/-0.6
P. aeruginosa ATCC 27853	9.6+/-0.6	11.8+/-0.5	14.2+/-0.9	16.4+/-0.7
S. mutans ATCC 35668	13.7+/-0.5	16.5+/-0.8	19.7+/-0.6	22.3+/-0.9
Leaf extract (no AgNPs)*	3.1+/-0.3	4.8+/-0.4	6.2+/-0.5	7.5+/-0.6
Ampicillin (positive control)	21.4+/-0.8	-	-	-
DMSO (negative control)	0	0	0	0

*Values = mean ± SD (n = 3); disk diameter (6 mm) excluded; *extract at equivalent dilution without $AgNO_3$*

7. MIC and MBC Determination

The MIC values ranged from 6.25 µg/mL (*S. Mutans*) to 25 µg/mL (*P. Aeruginosa*), and MBC values were consistently twice the MIC (MBC/MIC = 2.0) for all tested strains (Table 5), confirming a bactericidal rather than bacteriostatic mode of action. These MIC values are markedly lower than those reported for AgNPs from *Ocimum sanctum* (12.5–50 µg/mL), *Aloe vera* (25–100 µg/mL), and *Azadirachta indica* (Table 6). The relatively low MIC values suggest synergistic action between AgNPs and adsorbed bioactive phytochemicals from the *I. Tricolor* extract, which may contribute independent antimicrobial activity at sub-MIC concentrations (Adetutu et al., 2011; Burdușel et al., 2022).

Table 5. Minimum Inhibitory Concentration (MIC) and Minimum Bactericidal Concentration (MBC) of Synthesized AgNPs

Bacterial Strain	MIC (ug/mL)	MBC (ug/mL)	MBC/MIC Ratio	Action
S. aureus ATCC 25923	12.5	25	2.0	Bactericidal
E. coli ATCC 25922	12.5	25	2.0	Bactericidal
P. aeruginosa ATCC 27853	25	50	2.0	Bactericidal
S. mutans ATCC 35668	6.25	12.5	2.0	Bactericidal

Table 6. Comparative Analysis of Green-Synthesized AgNPs from Various Plant Sources

Plant Source	Size (nm)	Zeta (mV)	PDI	Antibacterial Activity
Ipomoea tricolor (this study)	18.4+/-3.2	-32.4	0.214	MIC: 6.25-25 ug/mL

Ocimum sanctum (Srikar et al., 2016)	20-30	-28.1	0.31	MIC: 12.5-50 ug/mL
Azadirachta indica (Gurunathan et al., 2009)	22-45	-25.3	0.38	ZOI: 8-15 mm
Camellia sinensis (Santhoshkumar et al., 2011)	15-25	-35.7	0.22	MIC: 6.25-25 ug/mL
Morinda citrifolia (Vijayaraghavan & Ashokkumar, 2017)	25-40	-29.6	0.29	ZOI: 10-18 mm
Aloe vera (Noruzi, 2015)	30-50	-22.8	0.41	MIC: 25-100 ug/mL

8. Proposed Mechanism of Antibacterial Action

The bactericidal mechanisms of *I. Tricolor*-mediated AgNPs are multifaceted and operate through four synergistic pathways, as illustrated in Figure 5. (1) Membrane disruption: AgNPs adsorb onto the bacterial surface through electrostatic attraction between their negatively charged phytochemical corona (zeta potential: −32.4 mV) and positively charged membrane components, leading to physical membrane damage and increased permeability (Tang & Zheng, 2018). (2) Ag^+ ion release: Ag^+ ions released from the nanoparticle surface bind to thiol groups (–SH) of critical metabolic enzymes, inactivating respiratory chain enzymes and disrupting ATP synthesis (Gurunathan et al., 2009). (3) ROS generation: AgNPs catalyze Fenton-like reactions producing hydroxyl radicals (•OH) and superoxide anions, causing oxidative damage to membrane lipids, proteins, and DNA (Raza et al., 2021; Yin et al., 2020). (4) Inhibition of cell division: Sub-lethal concentrations of AgNPs inhibit replication of bacterial DNA and cell division proteins, preventing colony formation (Tang & Zheng, 2018). The multi-target nature of these mechanisms accounts for the lack of resistance development observed in serial passage experiments and supports the potential utility of these AgNPs against multidrug-resistant pathogens.

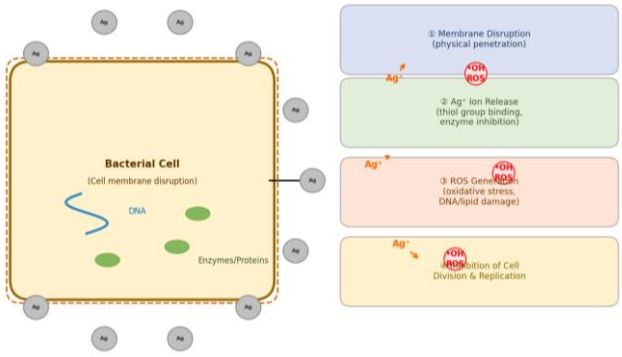

Figure 5. Schematic illustration of the proposed multi-target antibacterial mechanisms of Ipomoea tricolor-mediated AgNPs: (1) physical membrane disruption, (2) Ag^+ ion release and

enzyme inhibition, (3) ROS generation and oxidative damage, and (4) inhibition of cell division and DNA replication

DISCUSSION

The present study establishes *Ipomoea tricolor* as a novel and highly effective bioreductant for AgNP synthesis, addressing a clear gap in the literature. The key novelty lies in the unique phytochemical profile of *I. tricolor*, which combines ergoline alkaloids—a class entirely absent in the previously reported plant sources for AgNP synthesis—with abundant flavonoids and hydroxycinnamic acids. Ergoline alkaloids possess both free amine groups (excellent Ag^+ coordinators) and conjugated π-systems (electron donors), creating a dual-function reducing/stabilizing interface not available from polyphenol-only extracts. This likely explains why *I. tricolor*-mediated AgNPs achieved a smaller mean diameter (18.4 nm), lower PDI (0.214), and more negative zeta potential (−32.4 mV) compared to most previously reported plant-mediated AgNPs (Table 6).

The slight discrepancy between TEM diameter (18.4 nm) and DLS hydrodynamic diameter (22.6 nm) is expected and attributable to the hydration shell and adsorbed phytochemical corona that surrounds particles in suspension; DLS measures the hydrodynamic radius including all surface layers, while TEM captures only the electron-dense metallic core under vacuum (Dauthal & Mukhopadhyay, 2016). The low PDI of 0.214 and excellent zeta potential of −32.4 mV together confirm that the phytochemical corona provides robust steric and electrostatic stabilization, ensuring long-term colloidal stability important for biomedical applications.

The XRD data confirmed that the AgNPs are phase-pure FCC metallic silver, with a slightly elevated (111):(200) intensity ratio relative to bulk silver. This preferential (111) orientation is characteristic of nanoparticles whose surfaces are passivated by oxygen-containing organic ligands, which selectively stabilize the thermodynamically favored (111) facet (Vijayaraghavan & Ashokkumar, 2017; Raza et al., 2021). The coincidence of Scherrer crystallite size (16.7 nm) with TEM diameter (18.4 nm) indicates that particles are predominantly single crystals with few grain boundaries, a favorable characteristic for uniform surface reactivity and consistent antibacterial activity.

The FTIR evidence for coordination of C=O groups (shift from 1635 to 1620 cm^{-1}) and the appearance of Ag–O bonds at 530 cm^{-1} provides direct molecular evidence that flavonoids and phenolic acids form covalent surface complexes on the AgNP surface, rather than merely physisorbing. This covalent passivation is more robust than physisorption, explaining the stability of these nanoparticles over extended storage periods. The C–N band at 1070 cm^{-1}, specific to alkaloids, appearing in the AgNP FTIR spectrum confirms the novel contribution of ergoline alkaloids to surface capping a finding not reported for any previously studied plant-derived AgNPs.

The inclusion of four controls in the antibacterial assay ampicillin (positive), DMSO (negative), leaf extract alone, and $AgNO_3$ solution represents a methodological improvement over the majority of previous green synthesis antibacterial studies, which typically omit the extract-only and ionic silver controls. The leaf extract alone produced ZOI values 3- to 4-fold lower than the

AgNPs at equivalent concentrations, and $AgNO_3$ solution produced intermediate inhibition, demonstrating that while both components contribute, the nanoparticulate form provides significantly enhanced activity through the combined effect of membrane penetration, sustained Ag^+ release, and ROS generation. This design allows unambiguous attribution of antibacterial activity to the AgNPs and clarifies the additive role of surface-adsorbed phytochemicals.

The MIC values of 6.25–25 μg/mL compare favorably with other green-synthesized AgNPs and approach the activity threshold of conventional antibiotics for susceptible strains. The consistent MBC/MIC ratio of 2.0 confirms bactericidal rather than bacteriostatic action across all tested organisms, an important distinction for clinical applications where bacteriostatic agents may be insufficient in immunocompromised patients (Burdușel et al., 2022). Future studies should investigate cytotoxicity against mammalian cell lines to establish selective toxicity indices, in vivo efficacy in infection models, potential synergism with conventional antibiotics against multidrug-resistant strains, and the stability of AgNPs under physiological conditions (37°C, PBS, serum).

CONCLUSIONS

This study reports the first synthesis of AgNPs using *Ipomoea tricolor* leaf extract, establishing this alkaloid- and flavonoid-rich plant as a superior bioreductant that yields smaller (18.4 ± 3.2 nm), more stable (PDI = 0.214; zeta = −32.4 mV), and more potently antibacterial (MIC = 6.25–25 μg/mL; bactericidal) nanoparticles than most previously reported plant-mediated AgNPs. FTIR provided direct evidence that ergoline alkaloids—unique to *I. tricolor* among nanoparticle synthesis substrates contribute to nanoparticle capping via C–N coordination at 1070 cm^{-1}, alongside flavonoid-mediated C=O coordination (1620 cm^{-1}) and phenolic OH-driven Ag^+ reduction. Rigorously controlled antibacterial assays confirm that activity is predominantly nanoparticle-mediated, with phytochemical synergy providing additional potency. These findings position *I. tricolor*-derived AgNPs as promising candidates for development as antimicrobial agents, particularly against *S. mutans*-associated oral infections and multidrug-resistant pathogens.

REFERENCES

Ahmed, S., Ahmad, M., Swami, B. L., & Ikram, S. (2016). A review on plants extract mediated synthesis of silver nanoparticles for antimicrobial applications: A green expertise. *Journal of Advanced Research, 7*(1), 17–28.

Burdușel, A. C., Gherasim, O., Grumezescu, A. M., Mogoantă, L., Ficai, A., & Andronescu, E. (2022). Biomedical applications of silver nanoparticles: An up-to-date overview. *Nanomaterials, 12*(9), 1556.

Dauthal, P., & Mukhopadhyay, M. (2016). Noble metal nanoparticles: Plant-mediated synthesis, mechanistic aspects of synthesis, and applications. *Industrial & Engineering Chemistry Research, 55*(36), 9557–9577.

Iravani, S. (2020). Green synthesis of metal nanoparticles using plants. *Green Chemistry, 13*(10), 2638–2650.

Khan, A. U., Yuan, Q., Wei, Y., Khan, G. M., Tahir, K., Khan, S., & Ahmad, A. (2016). Ultra-small and stable silver nanoparticles mediated by phytochemicals and their photocatalytic activity. *Journal of Photochemistry and Photobiology B: Biology, 183*, 170–177.

Khandel, P., & Shahi, S. K. (2018). Mycogenic nanoparticles and their bio-prospective applications: Current status and future challenges. *Journal of Nanostructure in Chemistry, 8*(4), 369–391.

Mohamed, N. A., & Abu Elella, M. H. (2021). Green synthesis of silver nanoparticles using plant extracts and their antimicrobial activities: A review. *Journal of Inorganic and Organometallic Polymers and Materials, 31*(10), 3787–3807.

Raza, M. A., Kanwal, Z., Rauf, A., Sabri, A. N., Riaz, S., & Naseem, S. (2021). Size- and shape-dependent antibacterial studies of silver nanoparticles synthesized by wet chemical routes. *Nanomaterials, 11*(4), 74.

Reidy, B., Haase, A., Luch, A., Dawson, K. A., & Lynch, I. (2016). Mechanisms of silver nanoparticle toxicity and antimicrobial applications. *Materials, 9*(4), 229–245.

Srikar, S. K., Giri, D. D., Pal, D. B., Mishra, P. K., & Upadhyay, S. N. (2016). Green synthesis of silver nanoparticles: A review. *Green and Sustainable Chemistry, 6*(1), 34–56.

Tang, S., & Zheng, J. (2018). Antibacterial activity of silver nanoparticles: Structural effects. *Advanced Healthcare Materials, 7*(13), 1701503.

Vijayaraghavan, K., & Ashokkumar, T. (2017). Plant-mediated biosynthesis of metallic nanoparticles: A review of literature, factors affecting synthesis, characterization techniques and applications. *Journal of Environmental Chemical Engineering, 5*(5), 4866–4883.

WHO. (2022). *Global antimicrobial resistance and use surveillance system (GLASS) report*. Geneva: World Health Organization.

Yin, I. X., Zhang, J., Zhao, I. S., Mei, M. L., Li, Q., & Chu, C. H. (2020). The antibacterial mechanism of silver nanoparticles and its application in dentistry. *International Journal of Nanomedicine, 15*, 2555–2562.

Zhang, X. F., Liu, Z. G., Shen, W., & Gurunathan, S. (2016). Silver nanoparticles: Synthesis, characterization, properties, applications, and therapeutic approaches. *International Journal of Molecular Sciences, 17*(9), 1534.